Materials Science and Engineering C 38 (2014) 244–251

Contents lists available at ScienceDirect

Materials Science and Engineering C

journal homepage: www.elsevier.com/locate/msec

Depth and rate dependent mechanical behaviors for articular cartilage: Experiments and theoretical predictions

Li-Lan Gao [a,*], Chun-Qiu Zhang [a,*], Hong Gao [b], Zhi-Dong Liu [a], Peng-Peng Xiao [a]

[a] Tianjin Key Laboratory for Control Theory & Applications in Complicated Industry Systems, School of Mechanical Engineering, Tianjin University of Technology, Tianjin, PR China
[b] School of Chemical Engineering and Technology, Tianjin University, Tianjin, PR China

ARTICLE INFO

Article history:
Received 3 August 2013
Received in revised form 6 January 2014
Accepted 8 February 2014
Available online 15 February 2014

Keywords:
Articular cartilage
Depth-dependent
Loading rate dependent
Mechanical property
Optimized DIC technique
Constitutive model

ABSTRACT

An optimized digital image correlation (DIC) technique was applied to investigate the depth-dependent mechanical properties of articular cartilage and simultaneously the depth-dependent nonlinear viscoelastic constitutive model of cartilage was proposed and validated. The creep tests were performed with different stress levels and it is found that the initial strain and instantaneous strain increase; however the creep compliance decreases with the increase of compressive stress. The depth-dependent creep strain of cartilage was obtained by analyzing the images acquired using the optimized DIC technique. Moreover the inhomogeneous creep compliance distributions within the tissues were determined at different creep time points. It is noted that both creep strain and creep compliance with different creep times decrease from cartilage surface to deep. The depth-dependent creep compliance increases with creep time and the increasing amplitude of creep compliance decreases along cartilage depth. The depth-dependent and stress rate dependent nonlinear stress and strain curves were obtained for articular cartilage through uniaxial compression tests. It is found that the Young's modulus of cartilage increases obviously along cartilage depth from superficial layer to deep layer and the Young's modulus of different layers for cartilage increases with the increase of stress rate. The Poisson's ratio of cartilage increases along cartilage depth with given compressive strain and the Poisson's ratio of different layers decreases with the increase of compressive strain. The depth-dependent nonlinear viscoelastic constitutive model was proposed and some creep data were applied to determine the parameters of the model. The depth-dependent compressive behaviors of cartilage were predicted by the model and the results show that there are good agreements between the experimental data and predictions.

1. Introduction

Articular cartilage is the connective tissue covering the surface of subchondral bone in diarthrodial joints, providing a nearly frictionless surface for joint articulation and functioning to transmit loads, absorb shock and sustain daily loading histories. In activities of daily living, the cartilage is exposed to a wide range of loads up to 10 times body weight and is subjected to both static and dynamic load. Microscopically, the composition and structure of cartilage vary through the depth of the tissue [1–5]. In normal articular cartilage, the water content decreases from more than 80% at the surface to 65% in the deep zone. The concentration of proteoglycan (PG) content is relatively low in the superficial zone and increases to a higher value in the middle zone. The collagen fibrils are oriented parallel to the articular surface in the superficial zone and are perpendicular to the articular surface in the deep zone. The unique structure and composition of cartilage hint to the inhomogeneity and anisotropy of the tissue's mechanical properties. So it is significant to investigate inhomogeneous mechanical properties of articular cartilage considering the importance of cartilage in maintaining the mobility and quality of life of individuals.

Classical compression tests, utilizing unconfined compression, indentation, and confined compression on full-thickness cartilage samples were performed to determine mechanical properties of articular cartilage since the compressive load is a kind of important physiological load for cartilage [6,7]. However, test results were limited to bulk properties averaged over the test specimen volume. Recognizing the dramatic differences in composition, structure and mechanical properties of different layers for cartilage, the relations between the mechanical deformation and composition and structure of cartilage were studied under compressive load [8–11]. The compression tests of partial thickness cartilage samples had been conducted [12,13], which yielded to the characteristic differences in mechanical properties between cartilage samples, harvested from surface, middle and deep cartilage layers. The depth-dependent mechanical properties of cartilage were investigated preliminarily [14–16]. Chegini and Ferguson [14] simulated the time and depth dependent Poisson's ratio of cartilage by developing an inhomogeneous orthotropic fiber embedded biphasic model. Bell

* Corresponding authors. Tel.: +86 22 60214133.
E-mail addresses: gaolilan780921@163.com (L.-L. Gao), zhang_chunqiu@126.com (C.-Q. Zhang).

http://dx.doi.org/10.1016/j.msec.2014.02.009
0928-4931/

et al. [15] investigated the steady-state deformations of different layers for solid phase of articular cartilage based on the completely homogeneous, layered and isotropic, and layered and anisotropic models. Oliver et al. [16] found that the depth-dependent strain gradients were most pronounced for 5% off-set strain. Recently, an optimized digital image correlation (DIC) technique was applied to achieve the measurement of two-dimensional deformation fields and obtain some depth-dependent properties for cartilage under uniaxial compression [5,17]. Taken together, these experiments have provided the foundation for understanding inhomogeneous cartilage biomechanics and developing computational models. However there is still the need to better understand the depth-dependent properties and their influences on mechanical response.

Frequently, many theoretical models have been proposed to predict the mechanical behaviors of articular cartilage. In these models, the solid phase of cartilage was assumed to be a hyperelastic [18,19], quasi-linear viscoelastic [20] or continuum fiber reinforced medium [21–23]. Nonetheless it is well-known that cartilage macromolecules are polydisperse [24] and likely exhibit complex molecular interactions. Namely the solid phase of cartilage is a nonlinear viscoelastic medium. Additionally, these models were able to explain the average time dependent, but not depth-dependent mechanical behaviors of cartilage. Hence the depth-dependent nonlinear viscoelastic characteristic needs to be incorporated in the constitutive law of cartilage which shows the flow-independent contribution to cartilage viscoelasticity.

In this study, the optimized DIC technique was applied to investigate the depth and loading rate dependent mechanical properties for articular cartilage through creep tests and uniaxial compression tests with different stress rates. The depth-dependent creep compliance of cartilage at different creep time points was obtained under constant compressive stress. The Young's modulus and Poisson's ratio of different layers were determined for articular cartilage with different stress rates. A depth-dependent nonlinear viscoelastic constitutive model was proposed to predict the depth-dependent creep behaviors and uniaxial mechanical behaviors of cartilage under unconfined compression.

2. Experiments

Articular cartilage from about 8-month-old pig knee joint was obtained 4–6 h post-mortem from a local slaughterhouse. The eighteen full-thickness cartilage samples with subchondral bone were harvested from the trochlea sites of three joints by using the steel trephine with the trephine core axis perpendicular to the articular surface since the structured and flat samples, which can be compressed on the entire surface, were easier to be taken from the trochlea site than from the condyle site. These samples were made in a dimension of about 5.5 mm in length, 4 mm in width and 2 mm in thickness. The structure of cartilage can be divided into three distinct zones: superficial zone, middle zone and deep zone by microscopic examination. Before conducting experiment all samples were soaked in saline so as to maintain the humidity of cartilage.

An optimized digital image correlation technique was applied to measure the two-dimensional deformation fields for cartilage samples under unconfined compression by using the microscopic mechanical testing system as shown in Fig. 1. The essence of this technique is to automatically measure displacements by tracking the change in position of points on digitized images of the object's surface. The optimized digital image correlation requires a random pattern on the sample surface that can be readily identified in sequential images. This random pattern enables us to perform digital image correlation of sequential images that record the deformation of the sample. In this study the iron oxide nanoparticles with diameter of 50 nm, which were scattered and embedded in the cartilage sample profile by being pressed very gently under microscope, were used as fiducial markers for cartilage sample and the relative position of these nanoparticles gave rise to a random pattern on the sample surface. Fig. 2 shows the microscopic images of a section of cartilage sample before and after creep under unconfined compression. It is shown that the black particles are the iron oxide nanoparticles. The nanoparticle group, the smallest visible diameter of which is 2–3μm, is considered to be the reference point due to the agglomeration of particles. The deformations of different layers for cartilage can be observed before and after creep under unconfined compression as shown in Fig. 2.

The creep tests were conducted at given stress levels under unconfined compression for cartilage specimens. Prior to any compressive loading the initial thickness of each sample was measured microscopically. The image of the sample in its load-free reference state was first acquired. The constant compressive stress levels of 0.1, 0.5 and 1 MPa were chosen by Ref. [25] and applied on three sets of independent samples at room temperature respectively and the creep time was 60 min. Simultaneously the cross sections of the compressed samples were imaged at a frame per second during the whole creep process and the images were analyzed using the optimized DIC technique to generate the displacement fields and strain fields. For each condition three samples were tested considering random error.

The uniaxial unconfined compression tests were carried out with different stress rates such as 0.0045, 0.045, 0.225 MPa/s at room temperature for three sets of independent cartilage specimens respectively and for each condition three samples were tested considering random error. Prior to any compressive loading the initial thickness of each sample was measured microscopically and the image of the sample was first acquired. The samples were also imaged during the whole compressing process and the images were analyzed using the optimized DIC technique to generate the displacement fields and the strain fields. The depth-dependent Young's modulus was investigated with different stress rates.

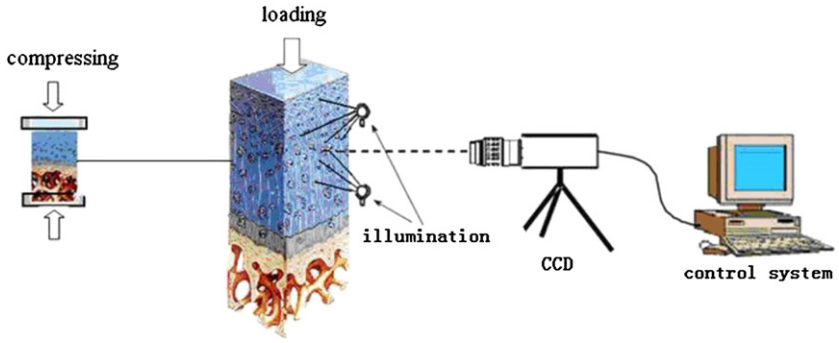

Fig. 1. Schematic diagram of the experimental system for cartilage under unconfined compression.

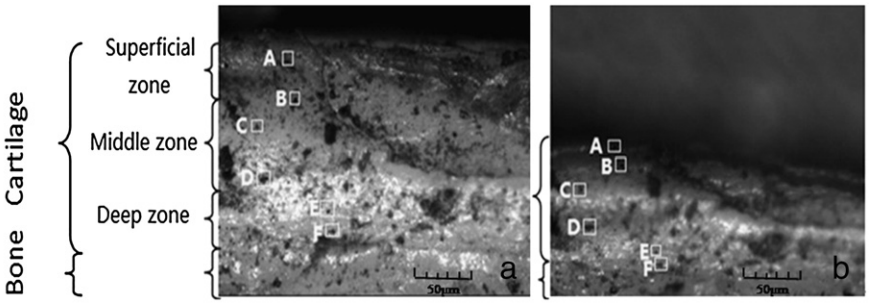

Fig. 2. Microscopic images of a section of cartilage sample before and after creep under unconfined compression.

3. Theoretical model

3.1. Derivation of depth-dependent constitutive model for cartilage

The articular cartilage was described by the following nonlinear viscoelastic constitutive equation for uniaxial loading by Onaran and Findley [26] and Lai and Findley [27] considering the nonlinear viscoelastic characteristic and complex molecular interactions of cartilage.

$$\varepsilon(t)=\int_0^t K_1(t\text{-}t_1)\dot{\sigma}(t_1)\mathrm{d}t_1+\int_0^t\int_0^t K_2(t\text{-}t_1,t\text{-}t_2)\dot{\sigma}(t_1)\dot{\sigma}(t_2)\mathrm{d}t_1\mathrm{d}t_2 +\int_0^t\int_0^t\int_0^t K_3(t\text{-}t_1,t\text{-}t_2,t\text{-}t_3)\dot{\sigma}(t_1)\dot{\sigma}(t_2)\dot{\sigma}(t_3)\mathrm{d}t_1\mathrm{d}t_2\mathrm{d}t_3 \quad (1)$$

where the kernels K_1, K_2, and K_3 are functions of the material under consideration, ε is the strain, t is the time, σ is the stress and $\dot{\sigma}(t)=\frac{\partial\sigma}{\partial t}$. To determine the Kernel functions, Eq. (1) is simplified with constant stress and the test data of constant-stress creep are used.

For creep deformation under constant stress, Eq. (1) becomes

$$\varepsilon(t)=K_1(t)\sigma+K_2(t)\sigma^2+K_3(t)\sigma^3 \quad (2)$$

The creep strain $\varepsilon(t)$ at constant stress σ is supposed to satisfy the power law relation [28]

$$\varepsilon(t)=\varepsilon_0+\varepsilon_t t^n \quad (3)$$

Where

ε_0 is the initial strain that depends on the cartilage depth,
ε_t is the nominal instantaneous strain that depends on the cartilage depth,
n is a parameter.

Consistent with this representation, the kernel functions K_1, K_2 and K_3 can be expressed as

$$K_1(t)=\mu_1+\omega_1 t^n \quad K_2(t)=\mu_2+\omega_2 t^n \quad K_3(t)=\mu_3+\omega_3 t^n \quad (4)$$

By substituting Eq. (4) into Eq. (2) and comparing with Eq. (3), we obtain

$$\varepsilon_0=\mu_1\sigma+\mu_2\sigma^2+\mu_3\sigma^3 \quad (5)$$

$$\varepsilon_t=\omega_1\sigma+\omega_2\sigma^2+\omega_3\sigma^3 \quad (6)$$

Accordingly μ_1, μ_2, μ_3, ω_1, ω_2 and ω_3 are the parameters that depend on the cartilage depth considering the depth-dependent ε_0 and ε_t. The relations of these parameters and normalized depth were fitted as the following respectively.

$$\mu_1=-22.71Z^2-1.93Z+49.97 \quad (7)$$

$$\mu_2=8.32Z^2+14.06Z-90.76 \quad (8)$$

$$\mu_3=-4.75Z^2-4.14Z+52.03 \quad (9)$$

$$\omega_1=41.64Z^2-78.19Z+42.33 \quad (10)$$

$$\omega_2=-104.3Z^2+191.2Z-101.1 \quad (11)$$

$$\omega_3=65.46Z^2-119.7Z+63.12 \quad (12)$$

where Z is the normalized depth which is the ratio of depth at a given location to total thickness of cartilage and $Z=0$ corresponds to the cartilage surface. Thus the depth-dependent nonlinear viscoelastic creep model named as NVC model is obtained based on Eqs. (2), (4) and (7)–(12).

Using the product form of these kernel functions K_1, K_2 and K_3 described by Eq. (4), the general Eq. (1) for strain history under varying prescribed stress becomes

$$\varepsilon(t)=\int_0^t\left[\mu_1+\omega_1(t\text{-}t_1)^n\right]\dot{\sigma}(t_1)\mathrm{d}t_1 +\int_0^t\int_0^t\left[\mu_2+\omega_2(t\text{-}t_1)^{n/2}(t\text{-}t_2)^{n/2}\right]\dot{\sigma}(t_1)\dot{\sigma}(t_2)\mathrm{d}t_1\mathrm{d}t_2 +\int_0^t\int_0^t\int_0^t\left[\mu_3+\omega_3(t\text{-}t_1)^{n/3}(t\text{-}t_2)^{n/3}(t\text{-}t_3)^{n/3}\right]\dot{\sigma}(t_1)\dot{\sigma}(t_2)\dot{\sigma}(t_3)\mathrm{d}t_1\mathrm{d}t_2\mathrm{d}t_3 \quad (1a)$$

Consequently the depth-dependent uniaxial mechanical behaviors of cartilage with different stress rates can also be predicted based on Eqs. (1a) and (7)–(12).

3.2. Determination of parameters

The parameters ε_0, ε_t and n are evaluated by the creep tests of cartilage with different constant stresses at room temperature based on Eq. (3), and n is found to be 0.31. The depth-dependent μ's and ω's are determined by Eqs. (5) and (6). Moreover the relations (7)–(12) are obtained by fitting the μ's and ω's with different normalized depths in terms of the least squares fit.

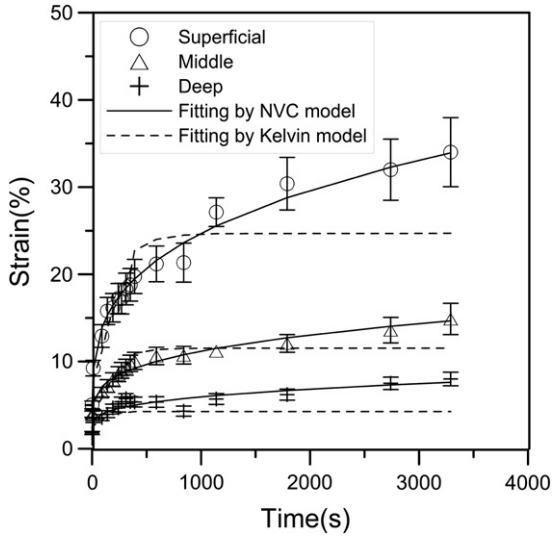

Fig. 3. Creep strain of different layers for cartilage with a compressive stress of 0.1 MPa.

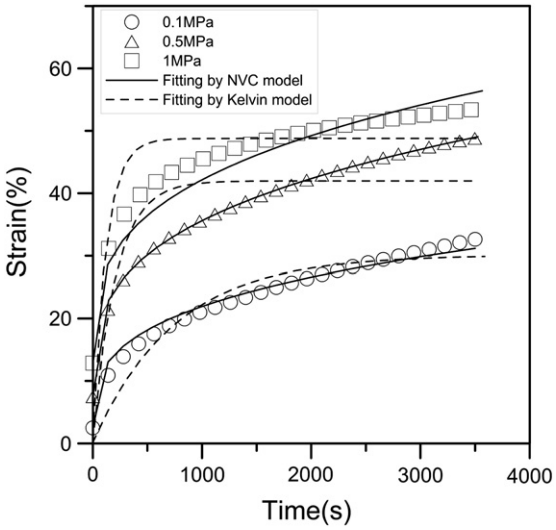

Fig. 5. Creep curves of cartilage with different compressive stress levels.

4. Results

4.1. Depth-dependent creep behaviors for articular cartilage with constant stress

The depth-dependent creep behaviors of cartilage were investigated with constant stress levels of 0.1, 0.5, and 1 MPa respectively and Fig. 3 shows the creep strain of different layers for cartilage with compressive stress of 0.1 MPa. It is found that the strain values of different layers increase with creep time. The creep strain and its increasing amplitude are the largest in superficial layer, and the creep strain and its increasing amplitude decrease along cartilage depth from surface to deep.

The depth-dependent creep behaviors of cartilage have also been fitted by the NVC model (Eqs. (2), (4) and (7)–(12)) proposed in this study and the Kelvin model by Ref. [29]. Fig. 3 shows the fittings of creep strain of different layers for cartilage with compressive stress of 0.1 MPa. It is noted that the fittings by the NVC model agree with the experimental data very well; however there are some differences between the fittings by the Kelvin model and experimental data.

Fig. 4 shows the depth-dependent creep compliance of cartilage with compressive stress of 0.1 MPa and creep time of 0, 200, 1000 and 3000 s by the tests and fittings of NVC model. It is found that the fittings agree with the experimental data very well. The creep compliance changes along cartilage depth and the creep compliance with different creep time decreases from cartilage surface to deep. The depth-dependent creep compliance increases with increasing creep time and the increasing amplitude of creep compliance decreases along cartilage depth. The increasing value of creep compliance from 0 s to 3000 s is 3.4 MPa^{-1} in cartilage surface; however it is 0.6 MPa^{-1} in cartilage deep.

4.2. Creep behaviors for articular cartilage with different compressive stress levels

Fig. 5 shows the creep curves of cartilage with different compressive stress levels. It is found that the initial strain and instantaneous strain increase with the increase of compressive stress. The creep rates with different compressive stresses are larger within creep time of 500 s and then decrease as the creep time goes by. The creep strains of cartilage with different compressive stress levels have also been fitted by the NVC model and Kelvin model. It demonstrates good agreement between the experimental data and fittings of NVC model as shown in

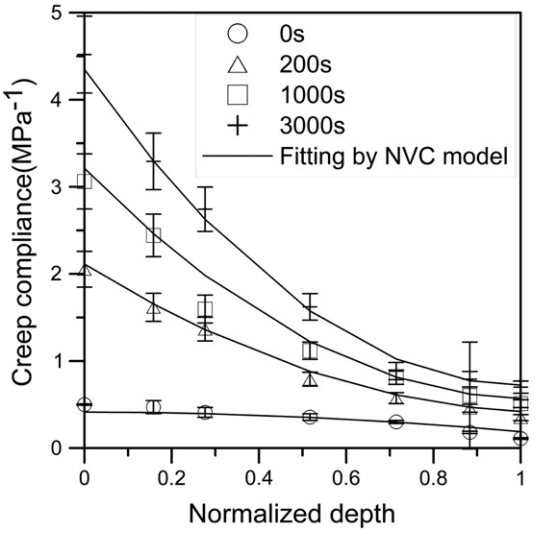

Fig. 4. Depth-dependent creep compliance of cartilage with different creep times and a constant compressive stress of 0.1 MPa.

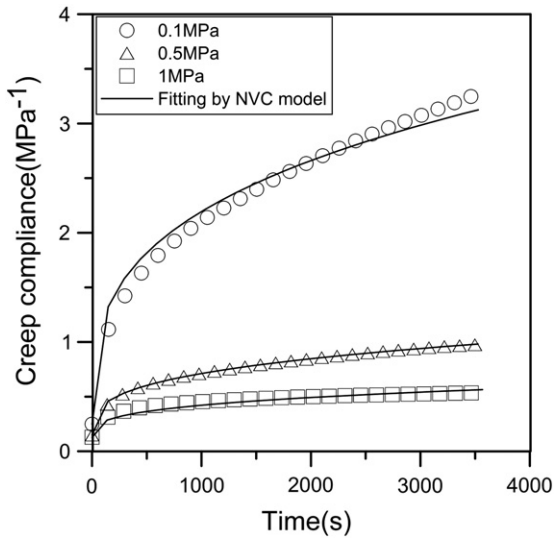

Fig. 6. Creep compliance curves of cartilage with different compressive stress levels.

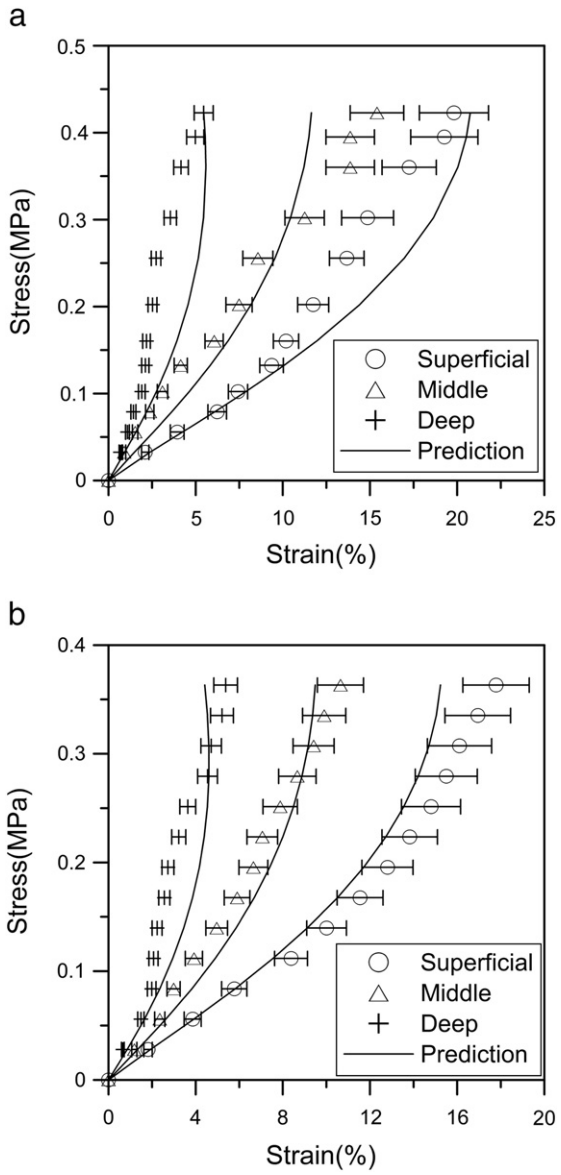

Fig. 7. Stress–Strain curves of different layers for cartilage with constant stress rate. (a) 0.0045 MPa/s; (b) 0.045 MPa/s.

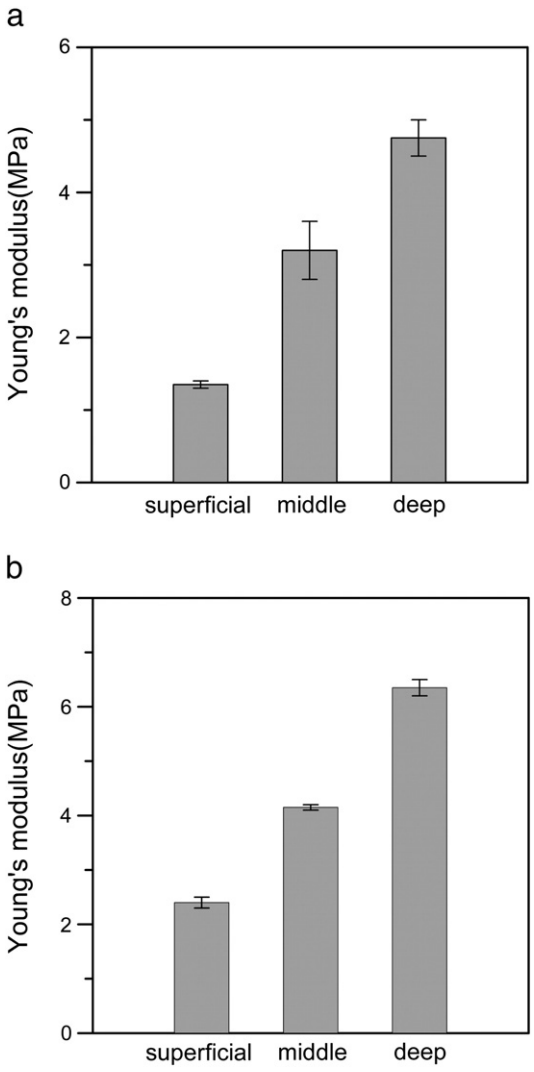

Fig. 8. Young's modulus of different layers for cartilage with a constant stress rate. (a) 0.0045 MPa/s; (b) 0.045 MPa/s.

Fig. 5; however some differences between the experimental data and fittings of the Kelvin model are observed in Fig. 5.

Fig. 6 shows the creep compliance curves of cartilage with different compressive stress levels by the tests and fittings of the NVC model (Eq. (2)). It is found that the fittings agree with the experimental data very well. It is also noted that the creep compliance increases rapidly first and then increases slowly as the creep progresses. The creep compliance decreases with the increase of compressive stress.

4.3. Depth-dependent compressive mechanical behaviors for articular cartilage with constant loading rate

The cartilage samples were compressed with constant stress rate at room temperature and the depth-dependent compressive mechanical behaviors for cartilage were investigated. Fig. 7(a) and (b) shows the stress–strain curves of different layers for cartilage with stress rates of 0.0045 MPa/s and 0.045 MPa/s respectively. It is found that the stress–strain curves of different layers are not coincident, which means that there are differences about the mechanical properties of different layers for cartilage. The strain of the superficial layer is the largest, the strain of the deep layer is the smallest and the strain of the middle layer is between the superficial layer and the deep layer with given compressive stress as shown in Fig. 7. The stress–strain curves of different layers for cartilage with constant stress rate have also been predicted by the depth-dependent constitutive model (Eqs. (1a) and (7)–(12)) and it demonstrates agreement between the experimental data and the predictions as shown in Fig. 7.

Fig. 8 shows the Young's modulus of different layers with constant stress rate. The Young's modulus of cartilage increases obviously along cartilage depth from the superficial layer to the deep layer and the nearly 3.6 times difference between the superficial zone and deep zone is observed with the stress rate of 0.0045 MPa/s as shown in Fig. 8(a). It is also found that the Young's modulus of different layers for cartilage increases with the increase of stress rate.

To determine the depth-dependent Poisson's ratio of cartilage the strain components were averaged along the direction parallel to cartilage surface at different cartilage depths, to yield the averaged strains (including transverse strain and axial strain) that varied only along the depth direction.

Fig. 9 shows the changes of Poisson's ratio of different layers for cartilage with different compressive strains and constant stress rate of 0.045 MPa/s. It is found that the Poisson's ratio of cartilage increases obviously along cartilage depth from the superficial layer to the deep layer with given compressive strain. The Poisson's ratio of different

layers decreases with the increase of compressive strain and it is also noted that the decreasing amplitude of Poisson's ratio is maximum. in the superficial layer. However there is a slight decrease for the Poisson's ratio of deep layer.

4.4. Compressive mechanical behaviors for articular cartilage with different stress rates

The compressive mechanical behaviors for cartilage were investigated with different stress rates and Fig. 10 shows the relationships of stress and strain with different stress rates. It is found that the stress rate makes very remarkable influence on the compressive behaviors of cartilage because the rate of submolecule motion within the sample is smaller than the rate of employing force during a certain interval. The stress–strain curves of cartilage with different stress rates have also been predicted by the constitutive model (Eq. (1a)) and it demonstrates agreement between the experimental data and predictions as shown in Fig. 10.

5. Discussions

The unconfined compression, indentation, and confined compression tests on full-thickness cartilage samples have been good tools to determine material properties of nonlinear viscoelastic, anisotropic, and multi-phasic articular cartilage for a wide range of cartilage conditions and loading regimes. The confined manner is the better tool to investigate the mechanical behaviors of cartilage compared with the unconfined manner since the cartilage compression always occurs in a confined manner. However the DIC technique used in this study is limited to visual access to the measurement area, which in turn requires the loading of cartilage sample in unconfined compression. Thus the unconfined compression tests for the full-thickness cartilage samples with subchondral bone had been performed to investigate the depth-dependent compressive mechanical behaviors of cartilage considering the effects of stress (or strain) amplitude and stress rate in the present study now that the stress rate as well as stress (or strain) amplitude were important factors influencing the normal function of cartilage.

It is found that the creep strain under constant compressive stress is the largest in superficial layer and decreases along cartilage depth from surface to deep. This finding agrees with the results of Guilak et al. [30] and Oliver et al. [16]. Guilak et al. [30] used confocal microscopy to measure the degree of chondrocyte deformation in the superficial, middle, and deep layers of canine femoral cartilage and it was found that the deformation of superficial zone was greater compared with the middle and deep zones. Oliver et al. [16] found that the strain was significantly largest in the superficial layer and it was smallest in the deep layer for femoral and patellar cartilage with different off-set strains under unconfined compression by using the customized laser-based electronic speckle pattern interferometry system. The change of creep compliance has also been investigated along cartilage depth with different compressive stress levels in this study for the first time. The creep compliance for different creep time points decreases along cartilage depth from surface to deep with the given compressive stress level. The depth-dependent creep compliance increases with creep time and the increasing amplitude of creep compliance decreases along cartilage depth. The creep compliance of cartilage decreases with the increase of compressive stress.

Under compression, the load is supported by the interstitial fluid of cartilage initially. Due to the rapid outflow of interstitial fluid under compressive load the creep strain of cartilage increases quickly at initial creep stage. The burden of supporting compressive load is gradually shifted to the fibril network which then deforms since the flow of fluid driven by gradients in fluid pressure dissipates the pressure in the interstitial fluid. It is found that the increasing rate of creep strain decreases with creep time as shown in Fig. 5. On the other hand, the flow of interstitial fluid is regulated by the pore matrix of cartilage and the flow rate is restricted by the smallest pores which have the highest fibril density and tortuosity. Thus the anisotropic permeability of pore networks is determined and contributes to the non-uniform creep deformation of cartilage along depth. In this study, the initial strain of cartilage was 12.8% under constant compressive stress of 1 MPa; however the strain increased to 53.6% when creep time was 3600 s due to the creep of cartilage and loss of interstitial water as shown in Fig. 5. The main reason is that the interstitial water within the cartilage samples was lost heavily and irreversibly since the samples during creep tests were not soaked in saline. When the creep test finished, the cartilage structure may be destructed with large strain (such as 53.6%). However the corresponding research has not been completed and will be carried out in the future work.

Consistent with the finding of depth-dependent aggregate modulus [31,5], the present study shows that the Young's modulus exhibits an increase through the depth of cartilage and the magnitude of the modulus in the deep layer can be up to 3.6-fold higher than that in the superficial layer with stress rate of 0.0045 MPa/s by applying an optimized digital image correlation (DIC) technique. In addition, the change trend of Poisson's ratio along cartilage depth in this study is in

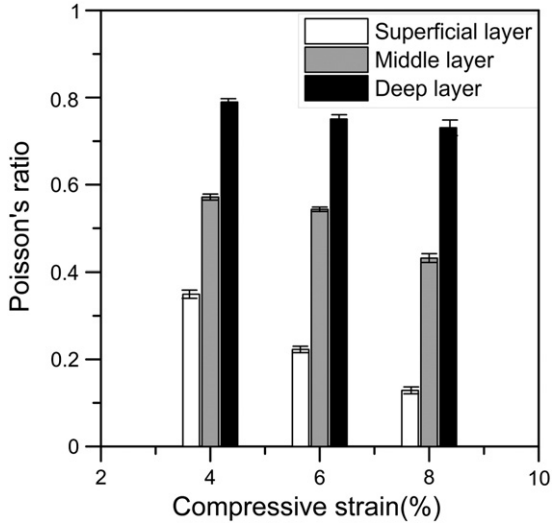

Fig. 9. Poisson's ratio of different layers for cartilage with different compressive strains and a constant stress rate of 0.045 MPa/s.

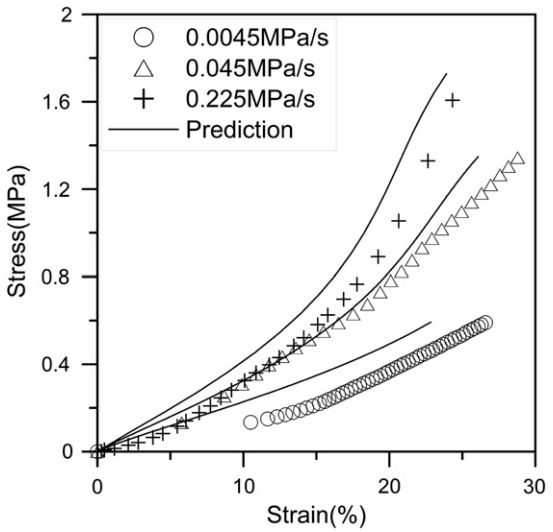

Fig. 10. Stress–Strain curves of cartilage with different stress rates.

relatively good agreement with that optically measured during unconfined compression [5] and fitted by FE model [14], where the Poisson's ratio of cartilage increases along cartilage depth from superficial layer to deep layer with given compressive strain. The interaction between the cartilage constituents is responsible for the depth-dependent Young's modulus and Poisson's ratio because the collagen fibers are activated in lateral tension and the depth-dependent PG concentration controls both the hydraulic permeability and axial compressive stiffness during unconfined compression [32]. Since the collagen fibrils of superficial zone are arranged parallel to the articular surface, this structural organization may produce the higher resistance to lateral expansion and the lower resistance to axial deformation. However the axial arrangement of fibrils in the deep zone may create a relatively low resistance to lateral expansion and a relatively high resistance to axial deformation. In addition, the monotonic increase of PG concentration along cartilage depth controls the same change trend of axial compressive stiffness. To sum up, the depth-dependent Young's modulus and Poisson's ratio of cartilage were determined.

However the Poisson's ratio of nearly 0.8 for the deep zone was obtained as shown in Fig. 9, which was greater than that of 0.3–0.6 for the deep zone of cartilage without subchondral bone [5,14]. It may be due to the influence of subchondral bone. The functioning joint, bonding of the cartilage layer to the subchondral bone, can restrict the lateral expansion of the deep layer of cartilage and strengthen the axial compressive stiffness of the deep layer of cartilage effectively. Thus the larger Poisson's ratio of deep layer may be the consequence of changes of lateral expansion and axial compressive stiffness influenced by the subchondral bone in that region.

Since the stress (or strain) rate is an important factor influencing the normal function of cartilage some research work has been done including the changes in biochemical composition and mechanical properties considering the effect of stress (or strain) rate [33,34]. However there are few reports about the effect of stress (or strain) rate on depth-dependent mechanical properties of cartilage. Our previous research work showed that the Young's modulus of cartilage increased along cartilage depth from surface to deep with the given strain rate and the Young's modulus of different normalized depth increases with the increase of strain rate [17]. The present work shows that the Young's modulus of cartilage increases obviously along cartilage depth and the Young's modulus of different layers for cartilage increases with the increase of stress rate. There are good agreements between two research achievements. It is also found that the stress rate makes very remarkable influence on the compressive behaviors of cartilage in terms of the stress–strain curves of cartilage with different stress rates as shown in Fig. 10.

The mechanical behaviors of cartilage can be predicted by the constitutive model. Historically, the constitutive model describing mechanical behaviors of cartilage is divided into the viscoelastic model and biphasic model since cartilage viscoelasticity has been separated into flow-independent and flow-dependent contributions. Leipzig and Kyriacos [35] found that the viscoelastic model showed excellent fitting for the majority of cartilage cells; however the biphasic model did not fit well for the initial creep response by comparing the unconfined creep compression data with the predictions of the viscoelastic model and the biphasic model. June et al. [36] found that the viscoelastic model best described the data from 1 to 100 s relaxation and the biphasic model best described the data from 100 s to equilibrium for cartilage. On the whole both the viscoelastic and biphasic models are able to predict the average time dependent, but not depth-dependent mechanical behaviors of cartilage. So the depth-dependent characteristic needs to be incorporated in the constitutive law of cartilage. Christopher et al. [31] predicted the depth-dependent stress relaxation behavior of articular cartilage in compression by incorporating the inhomogeneous aggregate modulus into the biphasic theory. The inhomogeneous relaxation modulus of cartilage was predicted by incorporating the depth-dependent strain into the biphasic relaxation model in our previous work [17]. However the depth-dependent mechanical behaviors considering the effects of stress amplitude and stress rates have not been predicted based on the existing constitutive models. In this study the depth-dependent nonlinear viscoelastic constitutive models (including the NVC model) were proposed and the depth-dependent creep behaviors with different stress levels and the uniaxial compressive behaviors of cartilage with different stress rates were predicted by the models. In addition, the Kelvin model was used to fit the depth-dependent creep strains with different stress levels. The results show that the creep behaviors of cartilage can be fitted by the NVC model very well; however there are some differences between the experimental data and fittings of the Kelvin model as shown in Figs. 3 and 5, which demonstrate the nonlinear and viscoelastic character of cartilage. It is also noted that there are good agreements between the experimental data and predictions of the model proposed in the present study for the uniaxial compressive behaviors of cartilage with different stress rates.

6. Conclusions

This study elucidated the depth-dependent creep behaviors with different stress levels and uniaxial compressive properties with different stress rates for articular cartilage under unconfined compression by tests and theoretical predictions. The results show that the creep strain and creep compliance with different creep time decrease along cartilage depth from surface to deep. The depth-dependent creep compliance increases with creep time and the increasing amplitude of creep compliance decreases along cartilage depth. The creep compliance increases rapidly first and then increases slowly as the creep progresses and decreases with the increase of compressive stress. It is found that the Young's modulus of cartilage increases obviously along cartilage depth from the superficial layer to the deep layer and the Young's modulus of different layers for cartilage increases with the increase of stress rate. The Poisson's ratio of cartilage increases along cartilage depth with given compressive strain and the Poisson's ratio of different layers decreases with the increase of compressive strain. The depth-dependent nonlinear viscoelastic constitutive model was proposed to predict the depth-dependent uniaxial compressive behaviors of cartilage. The results show that there are good agreements between the experimental data and predictions.

Conflict of interest statement

There are no conflicts of interest for either author.

Acknowledgements

The project was partly supported by the National Natural Science Foundation of China (Nos. 31000422, 10872147 and 11172208) and the China Postdoctoral Science Foundation (No. 2012T50226).

References

[1] R.K. Korhonen, M. Wong, J. Arokoski, R. Lindgren, H.J. Helminen, E.B. Hunziker, J.S. Jurvelin, Med. Eng. Phys. 24 (2002) 99.
[2] A. Thambyah, N. Broom, J. Anat. 209 (2006) 611.
[3] X. Bi, G. Li, S.B. Doty, N.P. Camacho, Osteoarthritis Cartilage 13 (2005) 1050.
[4] W. Wilson, C.C.V. Donkelaar, B.V. Rietbergen, R. Huiskes, J. Biomech. 38 (2005) 1195.
[5] C.C.B. Wang, J.M. Deng, G.A. Ateshian, C.T. Hung, J. Biomech. Eng. 124 (2002) 557.
[6] P.M. Bursac, T.W. Obitz, S.R. Eisenberg, D. Stamenovic, J. Biomech. 32 (1999) 1125.
[7] M.R. DiSilvestro, J.K. Suh, J. Biomech. 34 (2001) 519.
[8] P. Julkunen, P. Kiviranta, W. Wilson, J.S. Jurvelin, R.K. Korhonen, J. Biomech. 40 (2007) 1862.
[9] P. Kiviranta, J. Rieppo, R.K. Korhonen, P. Julkunen, J. Töyräs, J.S. Jurvelin, J. Orthop. Res. 24 (2006) 690.
[10] P. Julkunen, W. Wilson, J.S. Jurvelin, J. Rieppo, C.J. Que, M.J. Lammif, R.K. Korhonenb, J. Biomech. 41 (2008) 1978.
[11] W.G. George, B. Zappone, O. Soderman, D. Topgaard, G. Rata, H. Zeng, J.N. Israelachvili, Biomaterials 31 (2010) 3117.
[12] R. Flachsmann, N.D. Broom, A.E. Hardy, J. Orthop. Res. 19 (2001) 1131.
[13] A.C. Chen, W.C. Bae, R.L. Schinagl, R.L. Sah, J. Biomech. 34 (2001) 1.
[14] S. Chegini, S.J. Ferguson, J. Biomech. 43 (2010) 1660.

[15] J.S. Bell, C.P. Winlove, C.W. Smith, H. Dehghani, Biomaterials 30 (2009) 6394.
[16] K.E. Oliver, B.R. John, W.E. Larry, B.S. Mark, M.M. Steven, B. Michael, J. Biomech. 38 (2005) 667.
[17] L.L. Gao, C.Q. Zhang, L.M. Dong, Y.W. Jia, Mater. Sci. Eng. C 32 (2012) 119.
[18] G.A. Ateshian, W.H. Warden, J.J. Kim, R.P. Grelsamer, V.C. Mow, J. Biomech. 30 (1997) 1157.
[19] C.Y. Huang, A. Stankiewicz, G.A. Ateshian, V.C. Mow, J. Biomech. 38 (2005) 799.
[20] C.Y. Huang, V.C. Mow, G.A. Ateshian, J. Biomech. Eng. 123 (2001) 410.
[21] W. Wilson, C.C. van Donkelaar, B. van Rietbergen, K. Ito, R. Huiskes, J. Biomech. 37 (2004) 357.
[22] J.J. Garcia, D.H. Cortes, J. Biomech. 39 (2006) 2991.
[23] L.P. Li, J.T. Cheung, W. Herzog, Med. Biol. Eng. Comput. 47 (2009) 607.
[24] M.W. Holmes, M.T. Bayliss, H. Muir, J. Biochem. 250 (1988) 435.
[25] T.T. Guo, J.J. Su, G.M. Li, 6th World Congress of Biomechanics (WCB 2010), 31, 2010, p. 919.
[26] K. Onaran, W.N. Findley, Trans. Soc. Rheol. 9 (1965) 99.
[27] J.S. Lai, W.N. Findley, Trans. Soc. Rheol. 12 (1968) 243.
[28] J.D.W.N. Findley, J.S. Lai, K. Onaran, North-Holland Pub Co., 1976.
[29] Meyers, Chawla, Prentice Hall, Inc., 1999.
[30] F. Guilak, A. Ratcliffe, V.C. Mow, J. Orthop. Res. 13 (1995) 410.
[31] C.B.W. Christopher, T.H. Clark, C.M. Van, J. Biomech. 34 (2001) 75.
[32] J.S. Jurvelin, M.D. Buschmann, E.B. Hunziker, J. Biomech. 30 (1997) 235.
[33] T. Quinn, R. Allen, B. Schalet, P. Perumbuli, E. Hunziker, ORS Trans. 25 (2000) 106.
[34] L.P. LiM, M.D. Buschmann, A. Shirazi-Adl, J. Biomech. Eng. 125 (2003) 161.
[35] N.D. Leipzig, A.A. Kyriacos, J. Biomech. 38 (2005) 77.
[36] R.K. June, C.P. Neu, J.R. Barone, D.P. Fyhrie, Mater. Sci. Eng. C 31 (2011) 781.